PAPER

Cytotoxicity and autophagy dysfunction induced by different sizes of silica particles in human bronchial epithelial BEAS-2B cells

Qiuling Li,[a,b] Hejing Hu,[a,b] Lizhen Jiang,[a,b] Yang Zou,[a,b] Junchao Duan*[a,b] and Zhiwei Sun*[a,b]

The adverse effects of silica nanoparticles are gaining attention due to their wide application in biomedicine. However, information about size-dependent toxicity induced by silica nanoparticles is insufficient. In this study, two size of nano-scale (40 nm, 60 nm) and one size of micro-scale (200 nm) silica particles were studied to investigate the possible mechanism of cytotoxicity and autophagy dysfunction in human bronchial epithelial BEAS-2B cells. The cell viability was decreased in a size- and dose-dependent manner, while the LDH activity, oxidative stress and mitochondrial damage significantly increased, induced by both nano- and micro-scale silica particles. Ultrastructural analysis showed that nano-scale silica particles could induce mitochondrial damage and autophagy, but not micro-scale particles. Verified by the autophagy inhibitor 3-MA, the expression of LC3 and SQSTM1/p62 was upregulated in nano-scale silica particles in a size- and dose-dependent manner, while the micro-scale particles had an inhibitory effect. In addition, autophagy activation and autophagy blockage were triggered by nano-scale silica particles *via* the PI3K/Akt/mTOR pathway. Our findings first demonstrated that exposure to nano-scale silica particles rather than micro-scale particles could lead to autophagy dysfunction and impair cellular homeostasis.

Introduction

Given that nanotechnology is being pioneered in the biomedical and biotechnological fields, consumer products that contain nanomaterials are widely used in our daily life.[1,2] According to the Project on Emerging Nanotechnologies (PEN), the top five engineered nanomaterials (ENMs) in nanotechnology-based consumer products are graphite, silver, silica, titanium dioxide and zinc.[3] Briefly: graphite nanoparticles are mainly used in sporting goods, and electronics and computers; silver nanoparticles are used in food and beverages, health and fitness, and home and garden; titanium dioxide nanoparticles are mostly applied in food and personal care products; and zinc nanoparticles have been used in remediation, optics, catalysis, and media recording. Among them, silica nanoparticles are commonly applied in cosmetics, food ingredients, and varnishes, as well as in drug delivery and bio-

imaging.[4–7] Yet, there are rising concerns about ENMs that have the potential to cause adverse biological effects and toxicological consequences.[8]

The growing applications of silica nanoparticles increase the hazards for human exposure and environmental systems. Thus, human beings could be exposed to silica nanoparticles to a great degree through inhalation, dermal penetration and digestion.[9] Generally, the inhalation route is a common method of uptake for nanoparticles.[10] *In vivo* studies found that silica nanoparticles could accumulate in the lung, induce bronchial epithelial cell proliferation and inflammation, and increase the number of bronchoalveolar lavage (BAL) cells, which is followed by fibrosis, emphysema and tissue damage.[11–13] When silica nanoparticles enter into the human body *via* inhalation, the bronchial epithelial cells will have first, unavoidable, contact with the particles. Thus, it is meaningful to explore the toxic effect and mechanism of silica nanoparticles on the bronchial epithelial cell line. Unfortunately, only a few studies reported that silica nanoparticles induced pro-inflammatory responses in lung epithelial cells *via* the p38/TACE/EGFR pathway.[14,15] The underlying mechanism is still unclear.

Autophagy is considered a novel molecular mechanism for nanomaterial-induced toxicity.[16,17] The basal level of auto-

[a]Department of Toxicology and Sanitary Chemistry, School of Public Health, Capital Medical University, Beijing 100069, P.R. China.
E-mail: jcduan@ccmu.edu.cn, zwsun@ccmu.edu.cn; Fax: +86 010 83911507;
Tel: +86 010 83911868, +86 010 83911507
[b]Beijing Key Laboratory of Environmental Toxicology, Capital Medical University, Beijing 100069, P.R. China

phagy is a cytoprotective mechanism to maintain cellular homeostasis; while a blockade in the autophagy flux can lead to autophagy dysfunction, resulting in severe pathological states and contributing to disease pathogenesis.[18,19] It was reported that several nanoparticles could induce autophagy and autophagic cell death, such as titanium dioxide nanoparticles, and iron and copper oxide nanoparticles,[20–22] whereas autophagy induced by ferroferric oxide nanoparticles supported a pro-survival mechanism in cells.[23] Yet, most studies focus on nanoparticles triggering the phenomenon of autophagy induction rather than the process of autophagy degradation. To some extent, whether the nanoparticles can be degraded is associated with the role of autophagy in the pro-survival or pro-death cellular process.

Since particle size is one of the most important characteristics in nanotoxicity research, different sizes (Nano-Si40, Nano-Si60 and Si200) of silica particles were researched in this study. A series of cytotoxicity and autophagy parameters were explored and the underlying mechanism for autophagy dysfunction was explored in human bronchial epithelial BEAS-2B cells. This will help gain an insight into size- and dose-dependent mechanisms of action and provide persuasive evidence in the safety evaluation of nanomaterials.

Materials and methods

Silica particles preparation and characterization

Silica particles were prepared and characterized using the Stöber method as described in our previous studies.[24,25] The particle size was increased by increasing the amount of the catalyst (NH_4OH) and silica precursor (tetraethyl orthosilicate, TEOS), and by decreasing the amount of water in the reaction mixture regardless of solvents used for the synthesis.[26] Briefly, 2.5 mL of TEOS was added to a premixed ethanol solution (50 mL) containing ammonia (2 mL) and water (1 mL). The reaction mixture was kept at 40 °C for 12 h with continuous stirring (150 rpm). The particles were isolated using centrifugation (12 000 rpm, 15 min) and rinsed three times with deionized water; after that, the particles were dispersed in deionized water (50 mL). The size and shape of the silica particles was observed under a transmission electron microscope (TEM) (JEOL JEM2100, Japan), and the size distribution study was performed using ImageJ software (National Institutes of Health, USA). The hydrodynamic size and zeta potential of the silica particles were detected with a Zetasizer (Malvern Nano-ZS90, Britain). The silica particles were dispersed using a sonicator for 5 minutes (160 W, 20 kHz,) (Bioruptor UDC-200, Belgium) prior to experimental use in culture medium, so as to minimize their aggregation.

Cell culture experiments and exposure to silica particles

The bronchial epithelial BEAS-2B cell line was purchased from the Cell Resource Center, Shanghai Institutes for Biological Sciences (SIBS, China). The cells were cultured in a humidified environment (37 °C, 5% CO_2), maintained in Dulbecco's Modified Eagle's Medium (DMEM) (Hyclone, USA) supplemented with 10% fetal bovine serum (Gibco, USA), 100 U mL^{-1} penicillin and 100 mg mL^{-1} streptomycin. For all experiments, the cells were seeded in culture plates at a density of 1×10^5 cells per mL to attach for 24 h, and then were treated with silica particles for 24 h. Suspensions of silica particles were dispersed using a sonicator (160 W, 20 kHz, 5 min) and diluted to various concentrations, then added to the BEAS-2B cells immediately. Control groups of cells were provided with an equivalent volume of DMEM without silica nanoparticles. Each group had five replicate wells.

MTT assay

The cell viability of the silica particles was determined using an MTT assay. Briefly, 1×10^4 BEAS-2B cells were seeded into a 96-well plate in 100 μL of DMEM and allowed to attach for 24 h at 37 °C. Then they were treated with the three kinds of silica particles (6.25, 12.5, 25, 50 and 100 μg mL^{-1}) for 24 h at 37 °C. Then 10 μL of MTT was added into each well at 5 mg mL^{-1} and incubated for 4 h. After 4 h incubation, 150 μL of dimethyl sulfoxide (DMSO) was added to each well and mixed thoroughly for 5 min. The optical density at 492 nm was measured with a microplate reader (Themo Multiscan MK3, USA).

Lactate dehydrogenase (LDH) assay

After BEAS-2B cells were treated with various concentrations (6.25, 12.5 and 25 μg mL^{-1}) of the three sizes of silica particles for 24 h, 100 μL of cell medium was used to measure lactate dehydrogenase (LDH) activity using an LDH Kit (Keygen, China), according to the manufacturer's instructions. The absorbance at 440 nm was measured using a UV-visible spectrophotometer (Beckman DU-640B, USA).

Autophagy observation using TEM

After the BEAS-2B cells were incubated for 24 h with the three kinds of silica particles (12.5 μg mL^{-1}), the cells were centrifuged at 2000 rpm for 10 min after washing with PBS to remove the supernatants. The cell samples were fixed in 3% glutaraldehyde. After leaving overnight, the samples were washed using 0.1 M PB three times, then post fixed with 4% osmium tetroxide for 3 h. After washing with distilled water, the samples were stained with 0.5% uranyl acetate for 1 h and underwent a serially dehydration processes with ethanol (30%, 60%, 70%, 90%, and 100%), after that, the samples were embedded in epoxy resin, being polymerized at 60 °C for 48 h. Ultrathin sections obtained with an ultramicrotome were stained using uranyl acetate and lead citrate. After air drying, these samples were observed using TEM (JEOL JEM2100, Japan).

Intracellular ROS measurements

The intracellular reactive oxygen species (ROS) levels were detected using 2′,7′-dichlorofluorescin diacetate (DCFH-DA) (Jiancheng, Nanjing, China). The BEAS-2B cells were treated with series concentrations (6.25, 12.5 and 25 μg mL^{-1}) of the

three sizes of silica particles for 24 h. According to the instructions, the cells in a 6-well plate were incubated in a 2 mL working solution of DCFH-DA at 37 °C for 30 min in the dark. Then the cells were washed three times with PBS and harvested. Fluorescence intensities correlating with the intracellular ROS quantities were measured using flow cytometry (Becton-Dickison, USA) at 488 nm excitation and 525 nm emission.

Detection of the mitochondrial membrane potential (MMP)

We detected the MMP using 5,5′,6,6′-tetrachloro-1,1′,3,3′-tetraethylbenzimidazolylcarbocyanide iodine (JC-1) (Sigma, USA). The ratio of green to red expresses the change in the MMP. The BEAS-2B cells were treated with series concentrations (6.25, 12.5 and 25 μg mL^{-1}) of the three sizes of silica particles for 24 h. Then the cells were washed with PBS and incubated with 10 μg mL^{-1} JC-1 for 20 min. After washing with PBS, the cells were analyzed using FCM (Becton-Dickison, USA). The green fluorescence intensity of the JC-1 monomer was determined at an excitation wavelength of 488 nm and an emission wavelength of 525 nm, whereas the red fluorescence intensity of the JC-1 polymer (J-aggregates) was determined at an excitation wavelength of 488 nm and an emission wavelength of 590 nm.

Western blot analysis

Briefly, the BEAS-2B cells were pretreated with or without 5 mM methyladenine (3-MA) for 1 h, then exposed to series concentrations of the three kinds of silica particles (6.25, 12.5 and 25 μg mL^{-1}) for 24 h. The BEAS-2B cells were washed with ice-cold PBS, and lysed in 1 mM phenylmethylsulfonyl fluoride (PMSF) (DingGuo, China), containing ice-cold RIPA lysis buffer and phosphatase inhibitor, for 30 min. After centrifuging the lysates at 15 000 rpm, at 4 °C for 15 min, the total protein was extracted with a Tissue Protein Rapid Extraction Kit (Keygen, China) and determined by performing a bicinchoninic acid (BCA) protein assay (DingGuo, China). Equal amounts of proteins (40 μg) were loaded onto 12–15% SDS-PAGE and electrophoretically transferred to polyvinylidene fluoride (PVDF) membranes (Millipore, USA). After blocking with 5% nonfat milk in Tris-buffered saline (TBS) containing 0.05% Tween-20 (TBST) for 1 h, the membrane was incubated with microtubule-associated protein 1 light chain 3β (LC3), P62, phosphoinositide 3-kinase (PI3K), p-PI3K, protein kinase B (Akt), p-Akt, the mammalian target of rapamycin (mTOR), and p-mTOR (1 : 1000, rabbit antibodies, CST, USA) overnight at 4 °C. Then the membrane was washed with TBST three times, and incubated with a horseradish peroxidase-conjugated anti-rabbit IgG secondary anti-body (CST, USA) for 1 h at room temperature. After washing three times with TBST, the antibody-bound proteins were detected using an ECL chemiluminescence reagent (Pierce, USA).

Statistical analysis

All data are expressed as mean ± the standard deviation. SPSS 22.0 software was used to perform the statistical analyses. We used Student's t-tests to analyze the comparison indicators between the treatment groups. Three or more treatment groups were compared by one-way analysis for multiple comparisons. The significant differences were considered at the level of $p < 0.05$.

Results

Characterization of silica particles

In the TEM images, the three classes of silica particles appeared well dispersed, with a spherical shape (Fig. 1A–C). We utilized the ImageJ software to measure the size distribution of the silica particles. The average diameters of the Nano-Si40, Nano-Si60 and Si200 particles were 41.26 nm, 61.51 nm, and 206.31 nm, respectively (Fig. 1a, 1b and 1c). The hydrodynamic sizes and zeta potentials of the silica particles were measured with DMEM as the culture medium and distilled water as the stock medium at different time points (Tables 1–3). Because of van der Waals forces and hydrophobic interactions with the surrounding media, silica particles usually have a larger hydrodynamic size than the original size in the dispersing medium. Zeta potentials provide quantitative information on the stability of the particles. Our results showed that the three sizes of silica particles (Nano-Si40, Nano-Si60 and Si200) had very good monodispersity and stability, both in distilled water and DMEM culture media.

Size- and dose-dependent cytotoxicity induced by silica particles

Cell viability was examined after the cultured cells were exposed to the three sizes of silica particles (Nano-Si40, Nano-Si60 and Si200) at various concentrations (6.25, 12.5, 25, 50, and 100 μg mL^{-1}) for 6 h, 12 h and 24 h. As shown in Fig. 2, the cell viability of BEAS-2B induced by Si200 and Nano-Si60 showed a significant change as early as the 25 μg mL^{-1} treated group at 24 h, and Nano-Si40 showed a significant change as early as the 12.5 μg mL^{-1} group. For the cell viability of the BEAS-2B cells after exposure to 25 μg mL^{-1} of the three sizes of silica particles, all the particles inhibited the cell viability, which decreased to 89.37% (Si200), 81.21% (Nano-Si60), and 60.47% (Nano-Si40) at 24 h. The LDH activity decreased after exposure to the three sizes of silica particles for 6 h, 12 h and 24 h for the BEAS-2B cells (Fig. 3). A significant difference in the LDH activity was observed for the 25 μg mL^{-1} treated group. The results showed the cell viability, induced by silica particles, gradually decreased in a size-, dose- and time-dependent manner.

Internalization and autophagy induced by silica particles

The TEM images showed that the cellular uptake of silica particles (Nano-Si40, Nano-Si60 and Si200) is strongly dependent upon particle size (Fig. 4). The uptake of particles by the BEAS-2B cells has a decreasing trend across the Nano-Si40, Nano-Si60 and Si200 treated groups. Autophagy induction triggered by silica particles (Nano-Si60, Nano-Si40) was observed
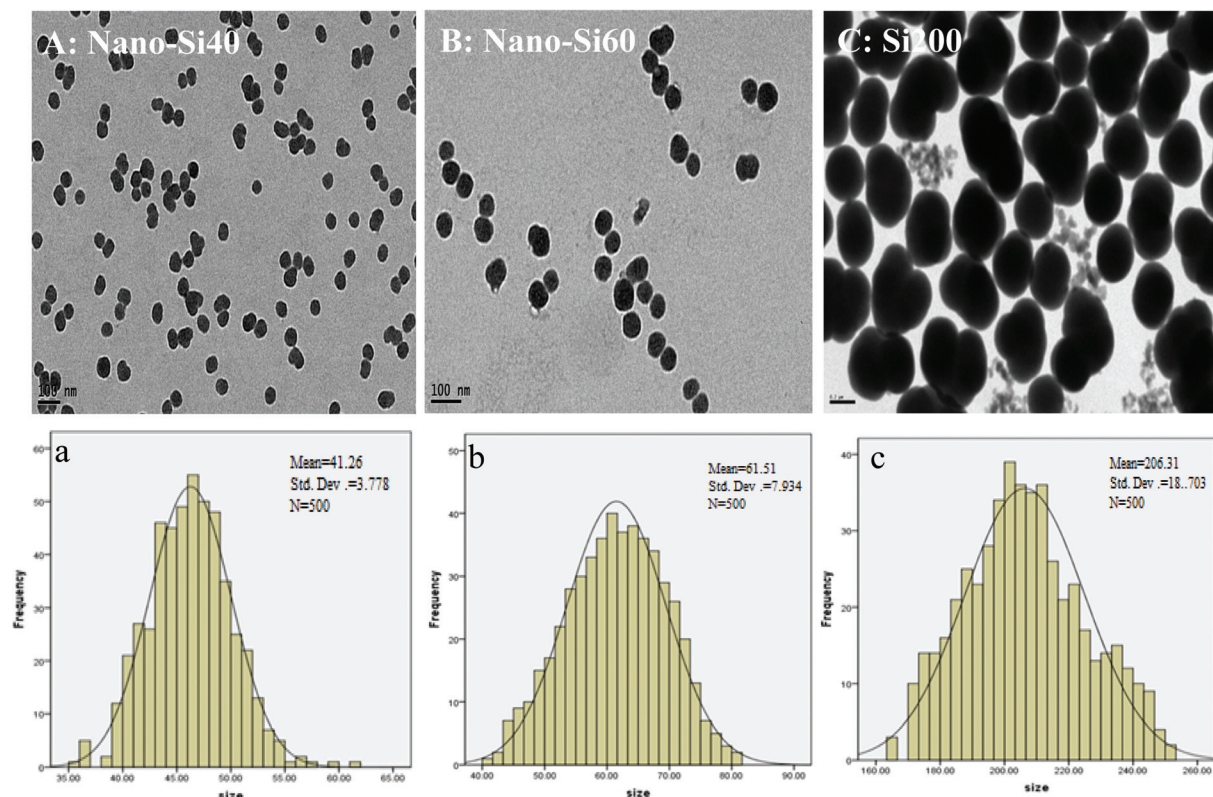
Fig. 1   Characterization of three different sizes of silica particles. The TEM images show silica particles with mean diameters of 41.26 ± 3.778 nm (A, a), 61.51 ± 7.934 nm (B, b), and 206.31 ± 18.703 nm (C, c). The size distribution of the silica particles, that was calculated using ImageJ software, showed an approximately normal distribution.

Table 1   Hydrodynamic size and zeta potential of silica particles (40 nm) in dispersion media

	Distilled water		Culture medium	
Time (h)	Diameter (nm)	Zeta potential (mV)	Diameter (nm)	Zeta potential (mV)
1	91.04 ± 0.71	−35.43 ± 0.67	92.54 ± 0.69	−34.03 ± 1.46
3	89.81 ± 0.32	−46.36 ± 0.55	96.50 ± 0.81	−32.47 ± 1.98
6	90.23 ± 1.11	−36.05 ± 0.78	97.28 ± 1.61	−36.57 ± 0.89
12	91.24 ± 2.07	−35.17 ± 1.46	95.36 ± 0.61	−30.80 ± 0.52
24	90.10 ± 0.86	−31.83 ± 2.76	94.38 ± 1.68	−35.23 ± 0.35
48	90.68 ± 0.89	−28.87 ± 1.32	97.56 ± 1.99	−28.87 ± 1.32

Data are expressed as mean ± S.D. from three independent experiments.

Table 2   Hydrodynamic size and zeta potential of silica particles (60 nm) in dispersion media

	Distilled water		Culture medium	
Time (h)	Diameter (nm)	Zeta potential (mV)	Diameter (nm)	Zeta potential (mV)
1	90.30 ± 1.49	−37.97 ± 0.55	92.54 ± 0.69	−34.60 ± 0.70
3	91.92 ± 1.32	−33.27 ± 1.33	93.82 ± 1.74	−31.40 ± 1.57
6	91.38 ± 1.08	−32.40 ± 2.36	94.99 ± 1.43	−32.27 ± 0.74
12	94.31 ± 1.57	−29.60 ± 1.11	99.56 ± 0.57	−34.00 ± 1.37
24	92.50 ± 1.10	−31.83 ± 2.76	95.64 ± 2.10	−34.20 ± 1.04
48	94.62 ± 2.08	−30.27 ± 1.60	98.79 ± 2.04	−33.30 ± 1.00

Data are expressed as mean ± S.D. from three independent experiments.

using ultrastructural analysis in Fig. 4C and D. The TEM images showed that the autophagic vacuoles contained degraded cytoplasmic contents, damaged mitochondria with swelling, cristae rupturing or disappearance, and highly electron-dense Nano-Si60 or Nano-Si40 in the BEAS-2B cells (Fig. 4c and d). Our data showed that the cellular uptake of silica particles is strongly dependent on particle size, and the Nano-Si60 and Nano-Si40 treated groups could induce mitochondrial damage and autophagy in BEAS-2B cells.

ROS generation and mitochondrial damage

As shown in Fig. 5A and a, all treated groups (Nano-Si40, Nano-Si60 and Si200) had a gradual increase in intracellular ROS after the BEAS-2B cells were exposed to silica particles for 24 h. The intracellular ROS levels in the Si200, Nano-Si60 and Nano-Si40 treated groups were elevated significantly compared to the control group. The MMP results showed the green/red ratios were increased after treating with a decreased size of silica particle (Si200, Nano-Si60 and Nano-Si40) (Fig. 5B and

Table 3 Hydrodynamic size and zeta potential of silica particles (200 nm) in dispersion media

Time (h)	Distilled water		Culture medium	
	Diameter (nm)	Zeta potential (mV)	Diameter (nm)	Zeta potential (mV)
1	199.83 ± 0.92	−51.90 ± 0.36	195.70 ± 1.05	−33.20 ± 0.70
3	199.57 ± 2.14	−52.37 ± 0.81	197.00 ± 2.09	−36.13 ± 0.55
6	197.43 ± 2.80	−57.80 ± 0.36	196.73 ± 1.17	−34.50 ± 1.65
12	201.23 ± 1.65	−50.50 ± 0.30	198.37 ± 1.06	−34.67 ± 1.11
24	201.93 ± 1.65	−54.63 ± 1.76	200.17 ± 0.15	−35.80 ± 1.01
48	200.83 ± 0.45	−53.57 ± 1.25	201.47 ± 0.96	−33.70 ± 0.95

Data are expressed as mean ± S.D. from three independent experiments.

b). In addition, all concentrations in the Nano-Si40 treated groups had significant differences compared with the control group. Our results demonstrated that silica particles induced ROS generation and mitochondrial damage in BEAS-2B cells in a size- and dose-dependent manner.

Autophagy dysfunction induced by silica particles

To confirm the autophagy dysfunction induced by the three sizes of silica particles (Si200, Nano-Si60 and Nano-Si40), we examined the protein marker of autophagy, LC3, and the auto-phagy degradation protein marker, p62 (also known as SQSTM1/sequestome 1). The relative densitometric analyses from Fig. 6 and 7 show that the protein levels of LC3-II/LC3-I and SQSTM1/p62 were upregulated in the Nano-Si60 and Nano-Si40 treated groups in a size-dependent manner, while the Si200 treated group had an inhibitory effect on LC3 and SQSTM1/p62. In regards to the dosage effect, LC3-II/LC3-I and SQSTM1/p62 were increased in a dose-dependent manner at 12.5 μg mL^{-1} and 25 μg mL^{-1} in the Nano-Si60 and Nano-Si40 treated groups, respectively. Our data shows that the nano-scale silica particles induce autophagy and impair autophagy degradation in a size-dependent manner, which indicates that silica nanoparticles could triggered autophagy dysfunction in BEAS-2B cells. To further confirm that autophagy played an important role in silica particle-triggered size-dependent toxicity, the autophagy inhibitor 3-MA was employed. As shown in Fig. 8, the protein expression of LC3-II/LC3-I and SQSTM1/p62 was significantly suppressed by 3-MA in a size-dependent manner.

Effects of silica particles on the PI3K/Akt/mTOR pathway

To further illustrate the underlying mechanisms of the silica particles (Nano-Si40, Nano-Si60 and Si200) on autophagy, we examined the PI3K/Akt/mTOR signaling pathway using western blot. The protein expressions of p-PI3K, p-Akt and
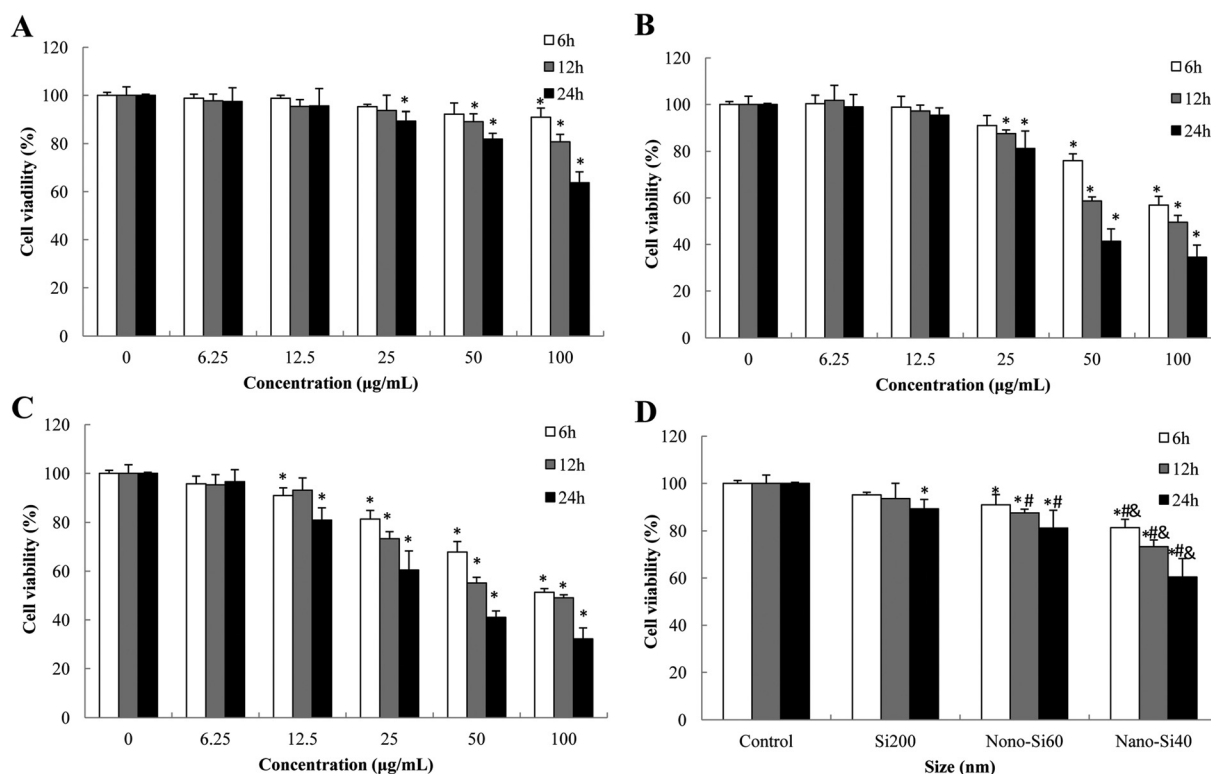

Fig. 2 Cell viability of BEAS-2B cells, induced by three sizes of silica particles, after 6 h, 12 h and 24 h exposure. Cell viability of BEAS-2B cells treated with Si200 (A), Nano-Si60 (B), and Nano-Si40 (C). (D) The cell viability of BEAS-2B cells after exposure to 25 μg mL^{-1} Si200, Nano-Si60, and Nano-Si40 silica particles. Data are expressed as mean ± S.D. *$p < 0.05$ compared with control group, #$p < 0.05$ compared with Si200 treated group, &$p < 0.05$ compared with Nano-Si60 treated group.
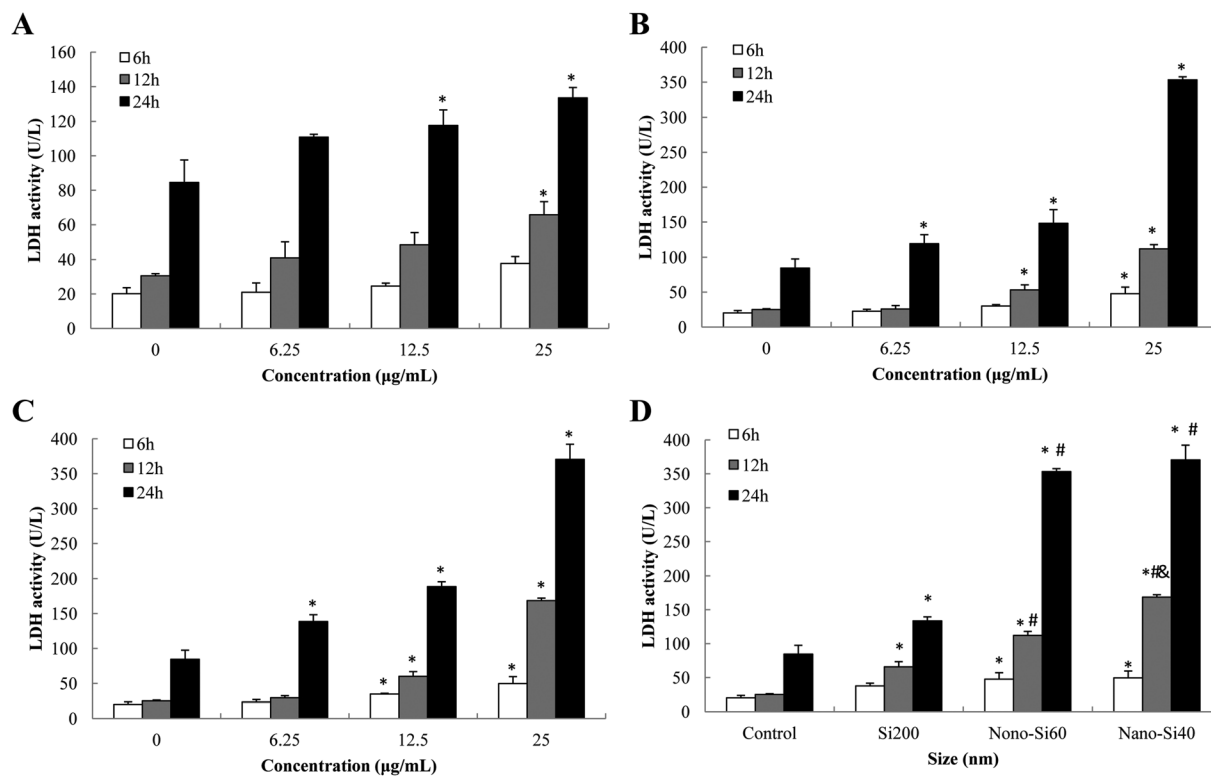
Fig. 3 LDH activity of BEAS-2B cells exposed to three sizes of silica particles at 6 h, 12 h and 24 h time points. (A, B, C) LDH activity of BEAS-2B cells treated with Si200, Nano-Si60, and Nano-Si40 silica particles at different concentrations (0, 6.25, 12.5, 25 μg mL^{-1}), respectively. (D) The LDH activity of BEAS-2B cells after exposure to 25 μg mL^{-1} Si200, Nano-Si60, and Nano-Si40 silica particles. Data are expressed as mean ± S.D. *$p < 0.05$ compared with control group, #$p < 0.05$ compared with Si200 treated group, &$p < 0.05$ compared with Nano-Si60 treated group.
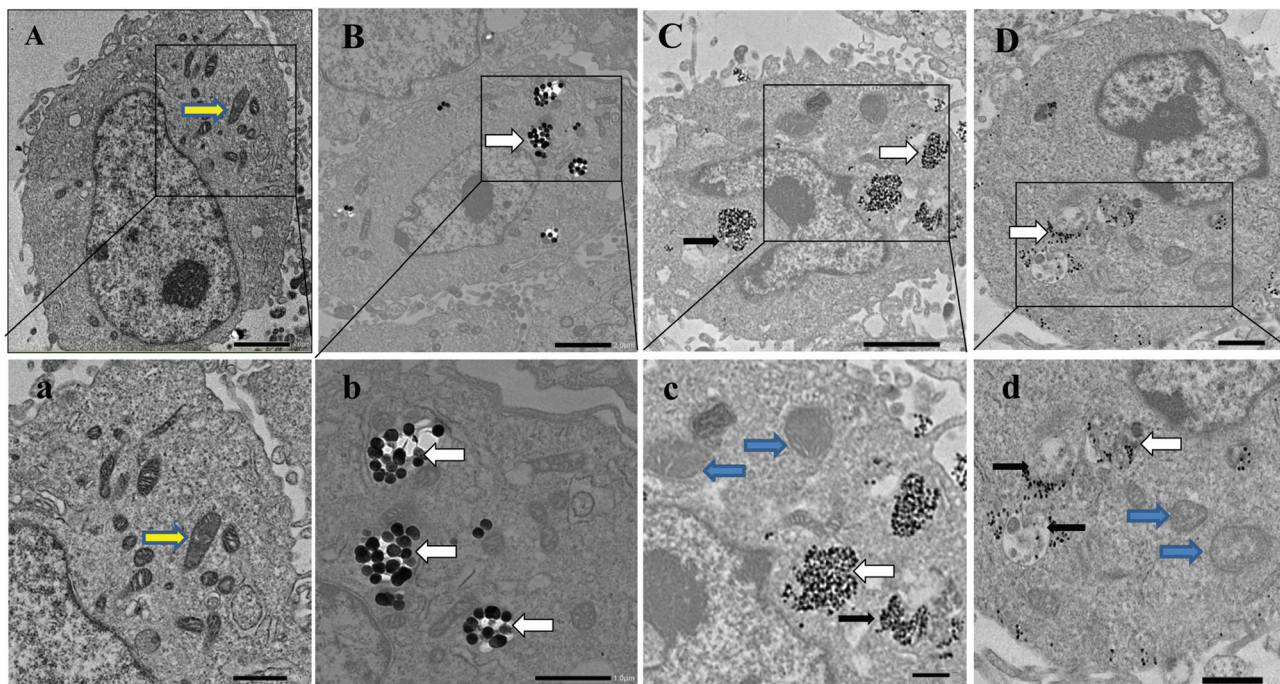

Fig. 4 TEM images of cellular uptake and autophagy induction for BEAS-2B cells exposed to the three sizes of silica particles using ultrastructural analysis. (A, a) Control group; (B, b) Si200; (C, c) Nano-Si60; and (D, d) Nano-Si40. Showing electron-dense silica particles dispersed in cytoplasm (white arrows). The magnification of the selected area shows evidently intact mitochondria (yellow arrows) in the control group, and mitochondrial swelling (blue arrows) induced by the Nano-Si60 and Nano-Si40 treated groups. The silica particles accumulated in autophagic vacuoles (black arrows) containing membrane-bound cytoplasmic material or degraded cytoplasmic materials. Scale bar: A, B, C, 2 μm; D, 1 μm; a, b, c, d, 1 μm.
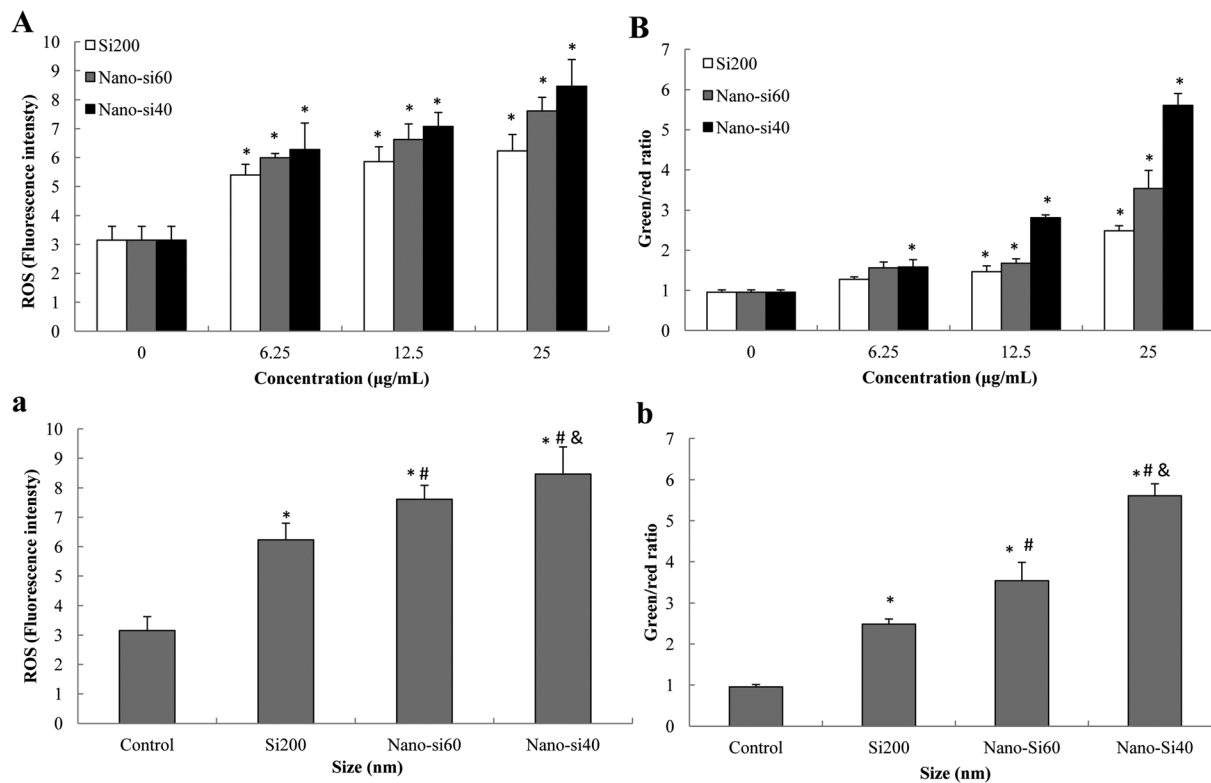
Fig. 5 Intracellular ROS and mitochondrial membrane potential (MMP), induced by three sizes of silica particles (Si200, Nano-Si60, Nano-Si40), in BEAS-2B cells. Intracellular ROS generation (A, a) and mitochondrial damage (B, b) in BEAS-2B cells treated with silica particles obviously increased in a size- and dose-dependent manner. Data are expressed as mean ± S.D. *$p < 0.05$ compared with control group, #$p < 0.05$ compared with Si200 treated group, &$p < 0.05$ compared with Nano-Si60 treated group.
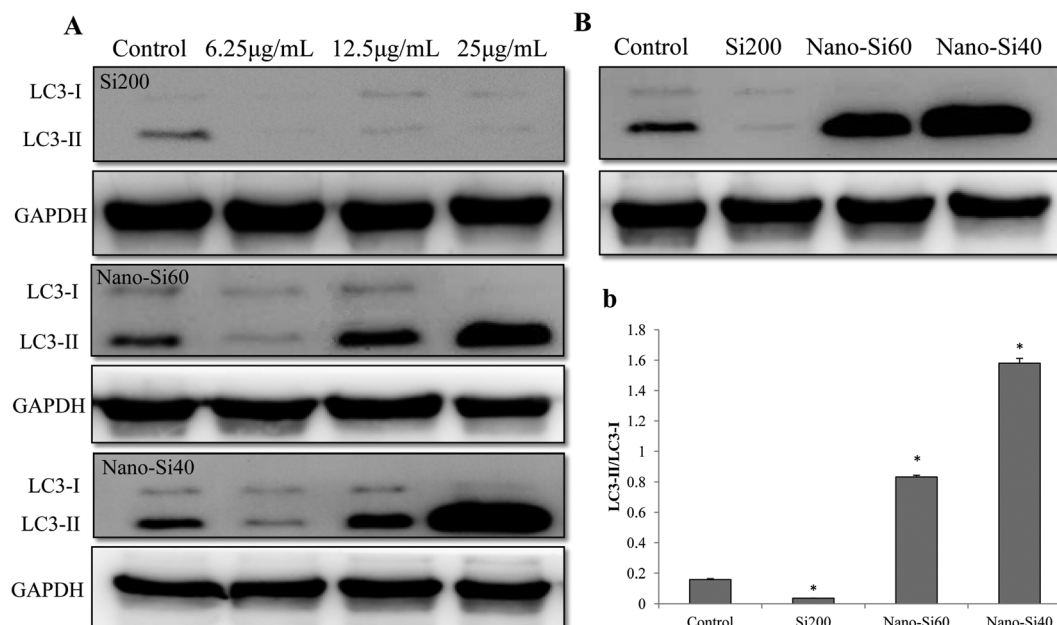

Fig. 6 Autophagy induction of BEAS-2B cells after exposure to three sizes of silica particles (Si200, Nano-Si60, Nano-Si40) measured using LC3-I/LC3-II conversion. (A) The expression of LC3 induced by different sizes of silica particles at concentrations of 6.25, 12.5, and 25 μg mL^{-1}. (B, b) The expression of BEAS-2B cells after exposure to 25 μg mL^{-1} of Si200, Nano-Si60, and Nano-Si40 silica particles. Data are expressed as mean ± S.D. *$p < 0.05$ compared with control group.
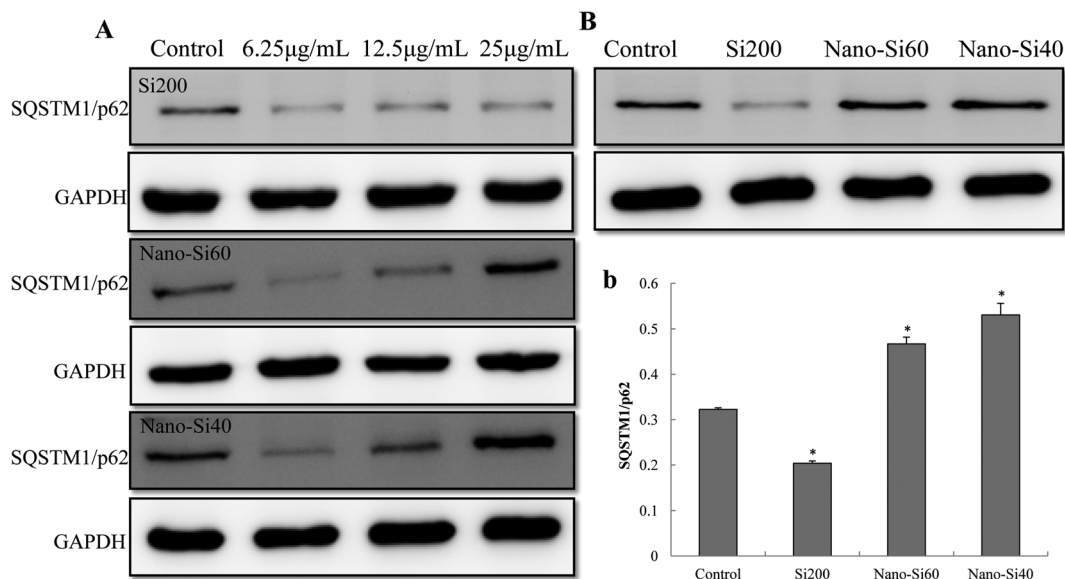
Fig. 7 Autophagy blockage of BEAS-2B cells after exposure to three sizes of silica particles (Si200, Nano-Si60, Nano-Si40) performed using SQSTM1/p62. (A) The expression of SQSTM1/p62 induced by different sizes of silica particles at concentrations of 6.25, 12.5, and 25 μg mL^{-1}. (B, b) The expression of BEAS-2B cells after exposure to 25 μg mL^{-1} of Si200, Nano-Si60, and Nano-Si40 silica particles. Data are expressed as mean ± S.D. * $p < 0.05$ compared with control group.

p-mTOR in BEAS-2B cells were significantly downregulated in a dose-dependent manner after exposure to different concentrations (0, 6.25, 12.5 and 25 μg mL^{-1}) of silica particles for 24 h (Fig. 9A–C). Results from Fig. 9D show that the protein expressions involved in the PI3K/Akt/mTOR pathway were markedly downregulated in the Nano-Si40 and Nano-Si60 treated groups, while there was no obvious change between the Si200 treated group and the control group. Our results indicate that nano-scale silica particles activated the PI3K/Akt/mTOR pathway in a size-dependent manner while micro-scale silica particles did not activate autophagy at the same concentration.

Discussion

Generally, a smaller size of nanoparticle is expected to possess greater surface area and higher biological activity compared to its micron-scale counterparts.[27] Although the size-dependent toxicity of silica nanoparticles was reported in several studies, the conclusions were still contradictory.[28,29] In the present study, two sizes of nano-scale silica particle (Nano-Si40, Nano-Si60) and one size of micro-scale silica particle (Si200) were studied to figure out whether the particle size affects the toxicological consequences. Our study demonstrated for the first time that nano-scale silica particles induce cytotoxicity and autophagy dysfunction in human bronchial epithelial BEAS-2B cells in a size- and dose-dependent manner, while micro-scale silica particles have an inhibitory effect on autophagy.

Firstly, the cell viability and LDH activity were measured in our study as indicators of cytotoxicity. The results demo-

nstrated that silica particles (Nano-Si40, Nano-Si60 and Si200) induced cytotoxicity in a size-, dose- and time-dependent manner (Fig. 2 and 3). Consistent with our study, size-dependent cytotoxicity was reported in several nanoparticles, such as silver, gold, copper oxide and iron oxide magnetic nanoparticles.[30–33] The internalization and localization of nanoparticles in cells were directly linked to biological effects and cytotoxicity. Our data showed that the cellular uptake of the three sizes of silica particles (Nano-Si40, Nano-Si60 and Si200) is strongly dependent upon particle size, and the Nano-Si40 and Nano-Si60 treated groups could induce mitochondrial damage and autophagy, while the autophagic vacuoles were not observed in the Si200 treated group with ultrastructural analysis (Fig. 4). Our previous study has found that nano-scale silica particles could induce autophagy in primary human umbilical vein endothelial cells (HUVECs) and human hepatocellular carcinoma HepG2 cells.[34,35] Thus, we could infer that the nano-scale silica particles had more potential to activate autophagy rather than micro-scale particles.

It was well-documented that mitochondrial damage was directly linked with autophagy induced by nanomaterials.[36,37] Our study found that the silica particles increased the mitochondrial depolarization and intracellular ROS in a size- and dose-dependent manner (Fig. 5). The mitochondrial hyperpolarization improves the organelles function, whereas mitochondrial depolarization can be removed by autophagy.[38] We suggested that silica particle-induced mitochondrial damage can occur directly from ROS generation due to the hydroxyl radicals (˙OH) released by the silica surface.[39,40] In line with our study, oxidative stress is the major mechanism for nanoparticle-caused toxicity *in vivo* or *in vitro*.[41,42] The pro-oxidant/
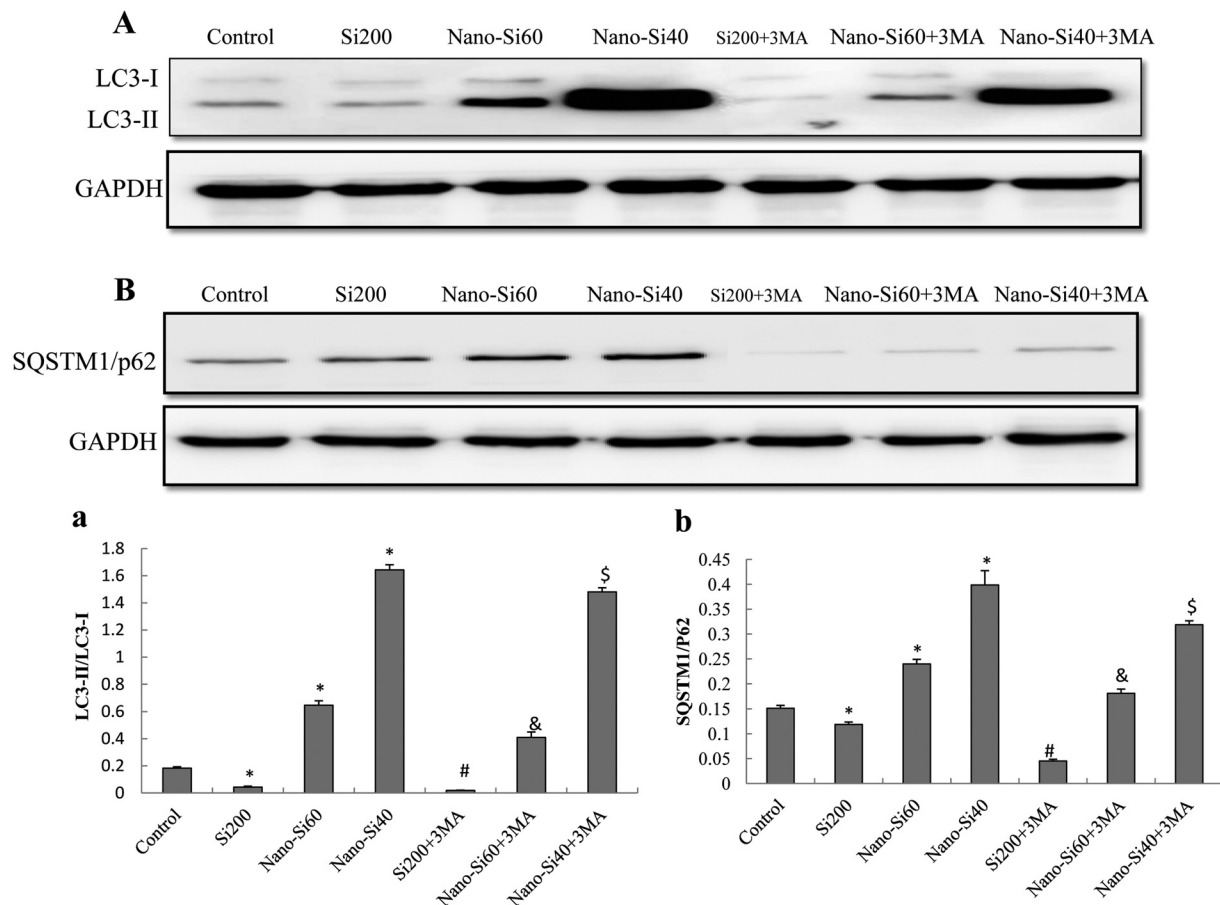
Fig. 8 Effect of silica particles (Si200, Nano-Si60, Nano-Si40) on autophagy marker LC3 and autophagy blockage marker SQSTM1/p62 by pre-treatment with the autophagy inhibitor, 3-MA. (A, a) The conversion of LC3-I to LC3-II markedly decreased by pre-treatment with 3-MA compared to treatment with the three sizes of silica particle alone. (B, b) The expression of SQSTM1/p62 declined obviously after pre-treatment with 3-MA compared to treatment with the three sizes of silica particle alone. Data are expressed as mean ±S.D. *$p < 0.05$ compared with control group, #$p < 0.05$ compared with Si200, &$p < 0.05$ compared with Nano-Si60, $$p < 0.05$ compared with Nano-Si40.

antioxidant imbalance results in an increasing of oxidative stress. The excess ROS generation could cause an impairment of biological macromolecules, such as the lipids, proteins and DNA, leading to the damage of several organelles, especially in mitochondria.[43,44] Recently, ROS-mediated autophagy is becoming a widely accepted paradigm of nanoparticle-induced autophagy.[45–47] Several environmental metal pollutants (*e.g.*, mercury, cadmium, and iron) were reported to induce autophagy *via* the response to ROS-mediated DNA damage and other molecular mechanisms.[48] For example, p38, but not JNK, was found to be involved in cadmium-induced autophagy.[49] Besides environmental pollutants, our previous study found that SiNP-induced autophagy and autophagy dysfunction contributed to apoptosis *via* p62 accumulation and negative regulation of the mTOR pathway.[50] In addition, prolonged exposure to SiNPs also induced cell death *via* pro-inflammatory action.[51] Further study is required to explore whether long-term exposure to SiNPs could trigger ROS-mediated autophagy.

Our data showed that the expression of LC3-II/LC3-I and SQSTM1/p62 was upregulated in the Nano-Si60 and Nano-Si40

treated groups in a size- and dose-dependent manner, while the Si200 treated group had an inhibitory effect on LC3 and SQSTM1/p62 (Fig. 6 and 7). This result relating to autophagy obtained in our study is not consistent with the cytotoxicity results. The Nomenclature Committee on Cell Death (NCCD) has classified that cell death can cover necrosis, apoptosis, autophagic cell death, mitotic catastrophe and other atypical modalities.[52] Our previous study had proved that silica nanoparticles (60 nm) could induce autophagic cell death.[53] Thus, we suggested that the micro-scale silica particles might induce cytotoxicity not through autophagic cell death, so the effects of Si-200 and Nano-Si40/60 on LC3 or p62 expression are opposite. That nano-scale silica particles, rather than micro-scale particles, could induce autophagy and blockade autophagy degradation was further verified using the autophagy inhibitor, 3-MA (Fig. 8). Since the activation of autophagy happens when the cytosolic LC3-I is converted into the enzymatic LC3-II, the LC3 protein is considered as an autophagy marker.[54] SQSTM1/p62, as a protein marker of autophagy blockage, is uniquely selectively downregulated in the complete process of
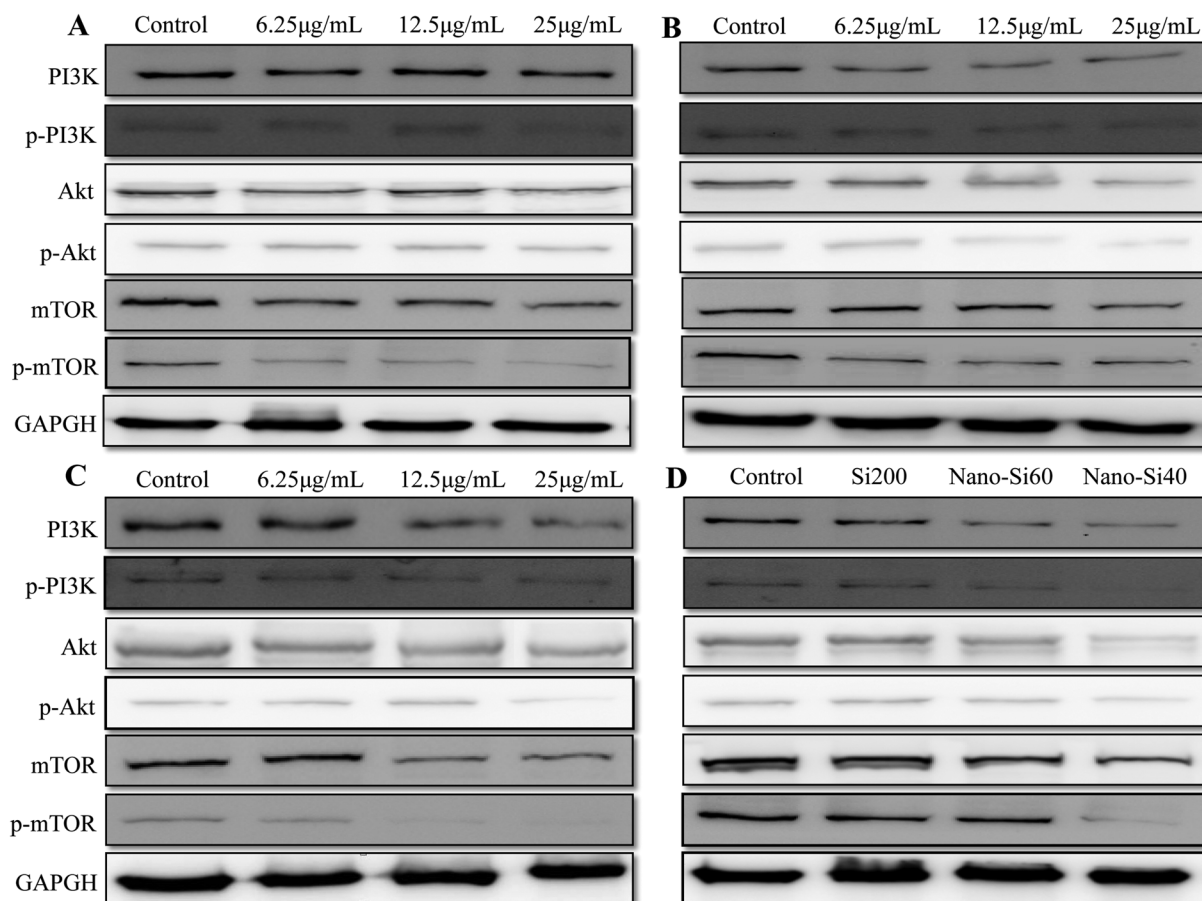
Fig. 9 Effects of silica particles (Si200, Nano-Si60, Nano-Si40) on the classical autophagy pathway PI3K/Akt/mTOR at different concentrations. A, Si200 treated group; B, Nano-Si60 treated group; C, Nano-Si40 treated group; and D, size dependence effect of silica particles on the PI3K/Akt/mTOR signaling pathway.

autophagy, or elevated in the case of a blockage in the autophagy flux.[55] Yet, autophagy is considered as a double-edged sword. Our data suggested that excessive autophagy and blocking of autophagy degradation could lead to autophagy dysfunction and disturb the cellular homeostasis.

To gain an insight into the underlying mechanism of autophagy dysfunction, autophagy-related proteins and the signaling pathway was measured using western blot analysis. Our results showed that the nano-scale silica particles (Nano-Si40 and Nano-Si60 treated groups) activated autophagy *via* the PI3K/Akt/mTOR signaling pathway in a size-dependent manner while micro-scale silica particles (Si200 treated group) did not activate autophagy at the same concentration (Fig. 9). It is well known that the PI3K/Akt/mTOR signaling pathway is a classical pathway involved in autophagy activation.[56] The rapamycin mTOR, a mammalian target, is critical in autophagy and the negative regulation of autophagy. Several studies including our findings have reported that autophagy is involved in nanoparticle-induced toxicity *via* the PI3K/Akt/mTOR pathway, such as in PAMAM nanoparticles, zinc oxide nanoparticles, poly-glycyrrhetinic acid nanoparticles, silver nanoparticles, and silica nanoparticles.[34,35,57–60] In addition, a

review summarized that PI3K, AKT, and mTOR are the major components of autophagy in the context of cellular responses to nanoparticles.[61] So we suggested that the PI3K/Akt/mTOR pathway could be a common mechanism for nanoparticle-induced autophagy. However, under our experimental conditions, we did not find the linkage between micro-scale silica particles and autophagy. More study is encouraged to investigate the relationship on this issue.

Conclusions

Using two nano-scale sizes (Nano-Si40 and Nano-Si60) and one micro-scale sizae (Si200) of silica particles, the present study demonstrated that silica particles induce cytotoxicity, oxidative stress and mitochondrial damage in a size- and dose-dependent manner in BEAS-2B cells. In addition, autophagy activation and autophagy blockage were triggered by nano-scale silica particles *via* the PI3K/Akt/mTOR pathway, while the micro-scale particles had an inhibitory effect on autophagy. Our findings suggest that exposure to nano-scale silica particles could lead to autophagy dysfunction and impair cellular

homeostasis. This will provide new evidence for the size-dependent toxicity of nanomaterials.

Conflict of interest

The authors declare they have no conflict of interest.

Acknowledgements

References

1 J. E. Hulla, S. C. Sahu and A. W. Hayes, Nanotechnology: History and future, *Hum. Exp. Toxicol.*, 2015, **34**, 1318–1321.

2 I. Iavicoli, V. Leso, W. Ricciardi, L. L. Hodson and M. D. Hoover, Opportunities and challenges of nanotechnology in the green economy, *Environ. Health*, 2014, **13**, 78.

3 S. F. Hansen, E. S. Michelson, A. Kamper, P. Borling, F. Stuer-Lauridsen and A. Baun, Categorization framework to aid exposure assessment of nanomaterials in consumer products, *Ecotoxicology*, 2008, **17**, 438–447.

4 F. Tang, L. Li and D. Chen, Mesoporous silica nanoparticles: Synthesis, biocompatibility and drug delivery, *Adv. Mater.*, 2012, **24**, 1504–1534.

5 X. Wu, M. Wu and J. X. Zhao, Recent development of silica nanoparticles as delivery vectors for cancer imaging and therapy, *Nanomedicine*, 2014, **10**, 297–312.

6 A. Weir, P. Westerhoff, L. Fabricius, K. Hristovski and N. von Goetz, Titanium dioxide nanoparticles in food and personal care products, *Environ. Sci. Technol.*, 2012, **46**, 2242–2250.

7 G. Madhumitha, G. Elango and S. M. Roopan, Biotechnological aspects of ZnO nanoparticles: overview on synthesis and its applications, *Appl. Microbiol. Biotechnol.*, 2016, **100**, 571–581.

8 P. C. Ray, H. Yu and P. P. Fu, Toxicity and environmental risks of nanomaterials: Challenges and future needs, *J. Environ. Sci. Health, Part C: Environ. Carcinog. Ecotoxicol. Rev.*, 2009, **27**, 1–35.

9 G. Oberdorster, A. Maynard, K. Donaldson, V. Castranova, J. Fitzpatrick, K. Ausman, J. Carter, B. Karn, W. Kreyling, D. Lai, S. Olin, N. Monteiro-Riviere, D. Warheit, H. Yang and Group IRFRSINTSW, Principles for characterizing the potential human health effects from exposure to nanomaterials: Elements of a screening strategy, *Part. Fibre Toxicol.*, 2005, **2**, 8.

10 C. L. Klein, K. Wiench, M. Wiemann, L. Ma-Hock, B. van Ravenzwaay and R. Landsiedel, Hazard identification of inhaled nanomaterials: Making use of short-term inhalation studies, *Arch. Toxicol.*, 2012, **86**, 1137–1151.

11 C. M. Sayes, K. L. Reed, K. P. Glover, K. A. Swain, M. L. Ostraat, E. M. Donner and D. B. Warheit, Changing the dose metric for inhalation toxicity studies: Short-term study in rats with engineered aerosolized amorphous silica nanoparticles, *Inhalation Toxicol.*, 2010, **22**, 348–354.

12 W. S. Cho, M. Choi, B. S. Han, M. Cho, J. Oh, K. Park, S. J. Kim, S. H. Kim and J. Jeong, Inflammatory mediators induced by intratracheal instillation of ultrafine amorphous silica particles, *Toxicol. Lett.*, 2007, **175**, 24–33.

13 J. H. Arts, M. A. Schijf and C. F. Kuper, Preexposure to amorphous silica particles attenuates but also enhances allergic reactions in trimellitic anhydride-sensitized brown norway rats, *Inhalation Toxicol.*, 2008, **20**, 935–948.

14 M. Gualtieri, T. Skuland, T. G. Iversen, M. Lag, P. Schwarze, D. Bilanicova, G. Pojana and M. Refsnes, Importance of agglomeration state and exposure conditions for uptake and pro-inflammatory responses to amorphous silica nanoparticles in bronchial epithelial cells, *Nanotoxicology*, 2012, **6**, 700–712.

15 T. Skuland, J. Ovrevik, M. Lag, P. Schwarze and M. Refsnes, Silica nanoparticles induce cytokine responses in lung epithelial cells through activation of a p38/tace/tgf-alpha/egfr-pathway and nf-kappabeta signalling, *Toxicol. Appl. Pharmacol.*, 2014, **279**, 76–86.

16 S. T. Stern, P. P. Adiseshaiah and R. M. Crist, Autophagy and lysosomal dysfunction as emerging mechanisms of nanomaterial toxicity, *Part. Fibre Toxicol.*, 2012, **9**, 20.

17 O. Zabirnyk, M. Yezhelyev and O. Seleverstov, Nanoparticles as a novel class of autophagy activators, *Autophagy*, 2007, **3**, 278–281.

18 A. M. Choi, S. W. Ryter and B. Levine, Autophagy in human health and disease, *N. Engl. J. Med.*, 2013, **368**, 1845–1846.

19 W. Martinet, M. W. Knaapen, M. M. Kockx and G. R. De Meyer, Autophagy in cardiovascular disease, *Trends Mol. Med.*, 2007, **13**, 482–491.

20 K. N. Yu, S. H. Chang, S. J. Park, J. Lim, J. Lee, T. J. Yoon, J. S. Kim and M. H. Cho, Titanium dioxide nanoparticles induce endoplasmic reticulum stress-mediated autophagic cell death via mitochondria-associated endoplasmic reticulum membrane disruption in normal lung cells, *PLoS One*, 2015, **10**, e0131208.

21 T. Sun, Y. Yan, Y. Zhao, F. Guo and C. Jiang, Copper oxide nanoparticles induce autophagic cell death in a549 cells, *PLoS One*, 2012, **7**, e43442.

22 M. I. Khan, A. Mohammad, G. Patil, S. A. Naqvi, L. K. Chauhan and I. Ahmad, Induction of ros, mitochondrial damage and autophagy in lung epithelial cancer cells by iron oxide nanoparticles, *Biomaterials*, 2012, **33**, 1477–1488.

23 M. Shi, L. Cheng, Z. Zhang, Z. Liu and X. Mao, Ferroferric oxide nanoparticles induce prosurvival autophagy in human blood cells by modulating the beclin 1/bcl-2/vps34 complex, *Int. J. Nanomed.*, 2015, **10**, 207–216.

24 J. Duan, Y. Yu, Y. Li, Y. Li, H. Liu, L. Jing, M. Yang, J. Wang, C. Li and Z. Sun, Low-dose exposure of silica nanoparticles induces cardiac dysfunction via neutrophil-mediated inflammation and cardiac contraction in zebrafish embryos, *Nanotoxicology*, 2015, 1–11.

25 J. Duan, Y. Yu, Y. Li, Y. Yu and Z. Sun, Cardiovascular toxicity evaluation of silica nanoparticles in endothelial cells and zebrafish model, *Biomaterials*, 2013, **34**, 5853–5862.

26 J. W. Kim, L. U. Kim and C. K. Kim, Size Control of Silica Nanoparticles and Their Surface Treatment for Fabrication of Dental Nanocomposites, *Biomacromolecules*, 2007, **8**(1), 215–222.

27 D. Napierska, L. C. Thomassen, B. Vanaudenaerde, K. Luyts, D. Lison, J. A. Martens, B. Nemery and P. H. Hoet, Cytokine production by co-cultures exposed to mono-disperse amorphous silica nanoparticles: The role of size and surface area, *Toxicol. Lett.*, 2012, **211**, 98–104.

28 W. Lin, Y. W. Huang, X. D. Zhou and Y. Ma, In vitro toxicity of silica nanoparticles in human lung cancer cells, *Toxicol. Appl. Pharmacol.*, 2006, **217**, 252–259.

29 E. Maser, M. Schulz, U. G. Sauer, M. Wiemann, L. Ma-Hock, W. Wohlleben, A. Hartwig and R. Landsiedel, In vitro and in vivo genotoxicity investigations of differently sized amorphous sio2 nanomaterials, *Mutat. Res., Genet. Toxicol. Environ. Mutagen.*, 2015, **794**, 57–74.

30 L. Yang, H. Kuang, W. Zhang, Z. P. Aguilar, Y. Xiong, W. Lai, H. Xu and H. Wei, Size dependent biodistribution and toxicokinetics of iron oxide magnetic nanoparticles in mice, *Nanoscale*, 2015, **7**, 625–636.

31 A. R. Gliga, S. Skoglund, I. O. Wallinder, B. Fadeel and H. L. Karlsson, Size-dependent cytotoxicity of silver nano-particles in human lung cells: The role of cellular uptake, agglomeration and ag release, *Part. Fibre Toxicol.*, 2014, **11**, 11.

32 W. H. De Jong, W. I. Hagens, P. Krystek, M. C. Burger, A. J. Sips and R. E. Geertsma, Particle size-dependent organ distribution of gold nanoparticles after intravenous administration, *Biomaterials*, 2008, **29**, 1912–1919.

33 A. Azam, A. S. Ahmed, M. Oves, M. S. Khan and A. Memic, Size-dependent antimicrobial properties of cuo nano-particles against gram-positive and -negative bacterial strains, *Int. J. Nanomed.*, 2012, **7**, 3527–3535.

34 J. Duan, Y. Yu, Y. Yu, Y. Li, J. Wang, W. Geng, L. Jiang, Q. Li, X. Zhou and Z. Sun, Silica nanoparticles induce autophagy and endothelial dysfunction via the pi3k/akt/mtor signaling pathway, *Int. J. Nanomed.*, 2014, **9**, 5131–5141.

35 Y. Yu, J. Duan, Y. Yu, Y. Li, X. Liu, X. Zhou, K. F. Ho, L. Tian and Z. Sun, Silica nanoparticles induce autophagy and autophagic cell death in hepg2 cells triggered by reactive oxygen species, *J. Hazard. Mater.*, 2014, **270**, 176–186.

36 H. Afeseh Ngwa, A. Kanthasamy, Y. Gu, N. Fang, V. Anantharam and A. G. Kanthasamy, Manganese nanoparticle activates mitochondrial dependent apoptotic signaling and autophagy in dopaminergic neuronal cells, *Toxicol. Appl. Pharmacol.*, 2011, **256**, 227–240.

37 Y. N. Wu, L. X. Yang, X. Y. Shi, I. C. Li, J. M. Biazik, K. R. Ratinac, D. H. Chen, P. Thordarson, D. B. Shieh and

F. Braet, The selective growth inhibition of oral cancer by iron core-gold shell nanoparticles through mitochondria-mediated autophagy, *Biomaterials*, 2011, **32**, 4565–4573.

38 D. R. Green, L. Galluzzi and G. Kroemer, Mitochondria and the autophagy-inflammation-cell death axis in organismal aging, *Science*, 2011, **333**, 1109–1112.

39 G. S. Shadel and T. L. Horvath, Mitochondrial ros signaling in organismal homeostasis, *Cell*, 2015, **163**, 560–569.

40 D. Napierska, L. C. Thomassen, D. Lison, J. A. Martens and P. H. Hoet, The nanosilica hazard: Another variable entity, *Part. Fibre Toxicol.*, 2010, **7**, 39.

41 M. Khatri, D. Bello, P. Gaines, J. Martin, A. K. Pal, R. Gore and S. Woskie, Nanoparticles from photocopiers induce oxidative stress and upper respiratory tract inflammation in healthy volunteers, *Nanotoxicology*, 2013, **7**, 1014–1027.

42 R. Alinovi, M. Goldoni, S. Pinelli, M. Campanini, I. Aliatis, D. Bersani, P. P. Lottici, S. Iavicoli, M. Petyx, P. Mozzoni and A. Mutti, Oxidative and pro-inflammatory effects of cobalt and titanium oxide nanoparticles on aortic and venous endothelial cells, *Toxicol. In Vitro*, 2015, **29**, 426–437.

43 M. Valko, D. Leibfritz, J. Moncol, M. T. Cronin, M. Mazur and J. Telser, Free radicals and antioxidants in normal physiological functions and human disease, *Int. J. Biochem. Cell Biol.*, 2007, **39**, 44–84.

44 L. Sun, Y. Li, X. Liu, M. Jin, L. Zhang, Z. Du, C. Guo, P. Huang and Z. Sun, Cytotoxicity and mitochondrial damage caused by silica nanoparticles, *Toxicol. In Vitro*, 2011, **25**, 1619–1629.

45 E. J. Park, D. H. Choi, Y. Kim, E. W. Lee, J. Song, M. H. Cho, J. H. Kim and S. W. Kim, Magnetic iron oxide nanoparticles induce autophagy preceding apoptosis through mitochondrial damage and er stress in raw264.7 cells, *Toxicol. In Vitro*, 2014, **28**, 1402–1412.

46 B. M. Johnson, J. A. Fraietta, D. T. Gracias, J. L. Hope, C. J. Stairiker, P. R. Patel, Y. M. Mueller, M. D. McHugh, L. J. Jablonowski, M. A. Wheatley and P. D. Katsikis, Acute exposure to zno nanoparticles induces autophagic immune cell death, *Nanotoxicology*, 2015, **9**, 737–748.

47 X. Feng, A. Chen, Y. Zhang, J. Wang, L. Shao and L. Wei, Central nervous system toxicity of metallic nanoparticles, *Int. J. Nanomed.*, 2015, **10**, 4321–4340.

48 S. Zhang, Z. Shang and P. Zhou, Autophagy as the effector and player in DNA damage response of cells to genotoxicants, *Toxicol. Res.*, 2016, **4**, 613–622.

49 K. Jung, H. Kim, B. Lee, S. Kim, K. So, T. An, H. Lee and S. Oh, Differential effects of p38 and JNK activation byGSK3 on cadmium-induced autophagy and Apoptosis, *Toxicol. Res.*, 2016, **4**, 976–985.

50 Y. Yu, J. Duan, Y. Yu, Y. Li, Y. Zou, Y. Yang, L. Jiang, Q. Li and Z. Sun, Autophagy and autophagy dysfunction contribute to apoptosis in HepG2 cells exposed to nanosilica, *Toxicol. Res.*, 2016, **5**, 871–882.

51 M. Mrakovcic, C. Meindl, E. Roblegg and E. Fröhlich, Reaction of monocytes to polystyrene and silicananoparticles

in short-term and long-termexposures, *Toxicol. Res.*, 2016, **3**, 86–97.

52 L. Galluzzi, I. Vitale, J. Abrams, E. Alnemri, E. Baehrecke, M. Blagosklonny, T. Dawson, V. Dawson, W. El-Deiry and S. Fulda, Molecular definitions of cell death subroutines: recommendations of the Nomenclature Committee on Cell Death 2012, *Cell Death Differ.*, 2011, **19**, 107–120.

53 Y. Yu, J. Duan, Y. Yu, Y. Li, X. Liu, X. Zhou, K. F. Ho, L. Tian and Z. Sun, Silica nanoparticles induce autophagy and autophagic cell death in HepG2 cells triggered by reactive oxygen species, *J. Hazard. Mater.*, 2014, **270**, 176–186.

54 I. Tanida, T. Ueno and E. Kominami, Lc3 and autophagy, *Methods Mol. Biol.*, 2008, **445**, 77–88.

55 S. Manley, J. A. Williams and W. X. Ding, Role of p62/sqstm1 in liver physiology and pathogenesis, *Exp. Biol. Med.*, 2013, **238**, 525–538.

56 J. O. Pyo, J. Nah and Y. K. Jung, Molecules and their functions in autophagy, *Exp. Mol. Med.*, 2012, **44**, 73–80.

57 C. Li, H. Liu, Y. Sun, H. Wang, F. Guo, S. Rao, J. Deng, Y. Zhang, Y. Miao, C. Guo, J. Meng, X. Chen, L. Li, D. Li, H. Xu, H. Wang, B. Li and C. Jiang, Pamam nanoparticles promote acute lung injury by inducing autophagic cell death through the akt-tsc2-mtor signaling pathway, *J. Mol. Cell Biol.*, 2009, **1**, 37–45.

58 R. Roy, S. K. Singh, L. K. Chauhan, M. Das, A. Tripathi and P. D. Dwivedi, Zinc oxide nanoparticles induce apoptosis by enhancement of autophagy via PI3K/Akt/mTOR inhibition, *Toxicol. Lett.*, 2014, **227**, 29–40.

59 F. Z. Wang, L. Xing, Z. H. Tang, J. J. Lu, P. F. Cui, J. B. Qiao, L. Jiang, H. L. Jiang and L. Zong, Codelivery of Doxorubicin and shAkt1 by Poly(ethylenimine)-Glycyrrhetinic Acid Nanoparticles To InduceAutophagy-Mediated Liver Cancer Combination Therapy, *Mol. Pharm.*, 2016, **13**, 1298–1307.

60 J. Lin, Z. Huang, H. Wu, W. Zhou, P. Jin, P. Wei, Y. Zhang, F. Zheng, J. Zhang, J. Xu, Y. Hu, Y. Wang, Y. Li, N. Gu and L. Wen, Inhibition of autophagy enhances the anticancer activity of silver nanoparticles, *Autophagy*, 2014, **10**, 2006–2020.

61 S. Chatterjee, S. Sarkar and S. Bhattacharya, Toxic metals and autophagy, *Chem. Res. Toxicol.*, 2014, **27**, 1887–1900.